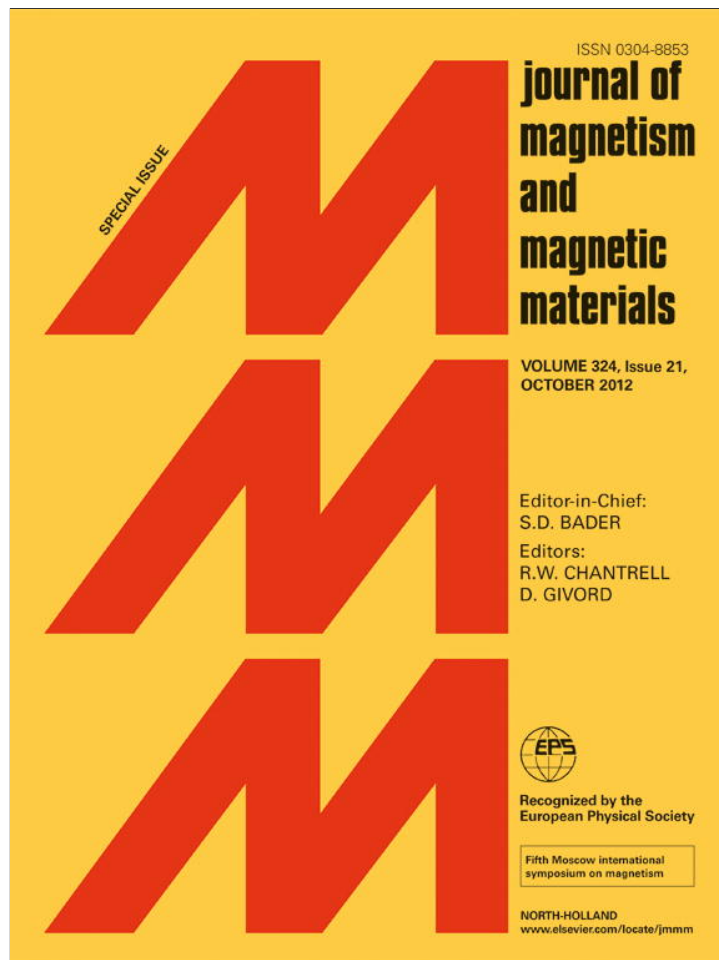


Provided for non-commercial research and education use.
Not for reproduction, distribution or commercial use.



This article appeared in a journal published by Elsevier. The attached copy is furnished to the author for internal non-commercial research and education use, including for instruction at the authors institution and sharing with colleagues.

Other uses, including reproduction and distribution, or selling or licensing copies, or posting to personal, institutional or third party websites are prohibited.

In most cases authors are permitted to post their version of the article (e.g. in Word or Tex form) to their personal website or institutional repository. Authors requiring further information regarding Elsevier's archiving and manuscript policies are encouraged to visit:

<http://www.elsevier.com/copyright>



Electrical control of ferromagnetic state

Leonid P. Rokhinson^{a,b,*}, Mason Overby^a, Alexandr Chernyshov^{a,1}, Yuli Lyanda-Geller^{a,b}, Xinyu Liu^c, Jacek K. Furdyna^c

^a Department of Physics, Purdue University, West Lafayette, IN 47907, USA

^b Birck Nanotechnology Center, Purdue University, West Lafayette, IN 47907, USA

^c Department of Physics, University of Notre Dame, Notre Dame, IN 46556, USA

ARTICLE INFO

Available online 27 February 2012

Keywords:

Ferromagnetic semiconductor

Spin polarization

Spin–orbit interaction

Multiferroic

ABSTRACT

We report experiments where magnetization in GaMnAs ferromagnetic semiconductor is manipulated via strain or electric current. In both cases, charge carrier holes become partially polarized due to the anisotropic modification of holes spectra caused by spin–orbit interactions, and this polarization exerts spin torque sufficient to rotate ferromagnetic domains.

© 2012 Elsevier B.V. All rights reserved.

1. Introduction

A rapidly developing field of spintronics is based on the idea that substituting charge with spin as a carrier of information can lead to new devices with lower power consumption, non-volatility and high operational speed [1]. While field detection using giant magnetoresistance (GMR) [2,3] and magnetic tunnel junctions (MTJ) [4] revolutionized readout heads in computer hard drives and magnetic memory [5], magnetization manipulation (the major advantage of active electronic devices) is trailing way behind. For example, current magnetic random access memory (MRAM) implementations rely on high currents to switch magnetization via Biot–Savart law, the process orders of magnitude less efficient than electrostatic gating in ordinary transistors. Spin-torque techniques [6,7] reduce switching currents by an order of magnitude, yet manipulation remains power-inefficient operation if compared with CMOS circuits.

Combining properties of semiconductor and ferromagnetic materials has been attempted in late 1970s [8,9]. However, the renewed interest in dilute magnetic semiconductors emerged after demonstration of $T_c \sim 100$ K in (Ga,Mn)As in late 1990s [10–12]. These materials were extensively studied both experimentally and theoretically over the past 15 years, see a recent review [13]. Unfortunately, despite serious efforts of many groups to increase T_c above the room temperature, the record T_c is still below 200 K. Nevertheless, (Ga,Mn)As can serve as an excellent prototype material where new functionality emerges from a combination of

semiconductor band structure, strong spin–orbit interactions and ferromagnetism, the combination that exposes new physics and enables the development of novel device concepts.

Straightforward electrostatic control of magnetization in (Ga,Mn)As proved to be limited. It has been shown that depletion of a ferromagnetic layer leads to a reduction in T_c [14,15]. This reduction comes from a simple fact that ferromagnetism in (Ga,Mn)As is carrier-mediated. In an elegant experiment, Chiba et al. [16] reported small angle rotation of magnetization vector. However, the true beauty of (Ga,Mn)As is hidden in a multiferroic nature of this material (both ferromagnetic and ferroelectric), which puts it in the same class as more exotic multiferroics like BiMnO₃ [17], BiCrO₃ [18], Bi₂NiMnO₆ [19]. Being ferroelectric, the (Ga,Mn)As lacks the center of inversion, and is characterized by strong spin–orbit (SO) coupling associated with lowered symmetry. Furthermore, hole spins are coupled to lattice deformation. In this work we show that magnetization direction in (Ga,Mn)As can be controlled via SO interaction [20] or external strain [21], both effects leading to partial polarization of current-carrying holes and the corresponding spin torque effect. The reported effects are different from the conventional spin-transfer torque, where polarized carriers are injected into ferromagnetic material and non-equilibrium polarization is limited to the interfacial layer. On the contrary, each carrier in (Ga,Mn)As generates its own effective magnetic field, which scales with volume.

2. Material and methods

The (Ga,Mn)As wafers (6–7% of Mn) were grown by molecular beam epitaxy at 265 °C on semi-insulating (001) GaAs

* Corresponding author at: Department of Physics, Purdue University, West Lafayette, IN 47907, USA.

E-mail address: leonid@purdue.edu (L.P. Rokhinson).

¹ Current address: Western Digital, San Jose, CA 95131.

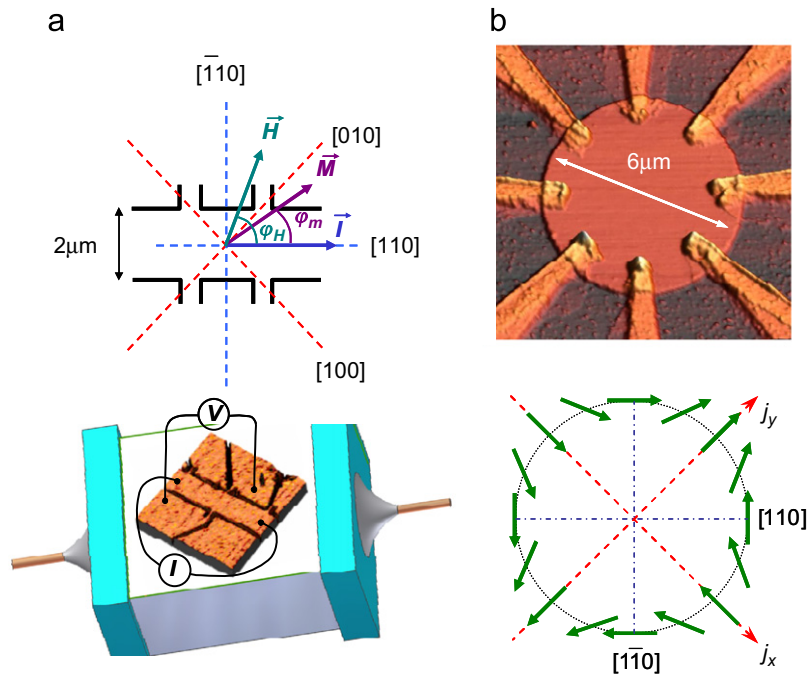


Fig. 1. Sample schematic for (a) strain and (b) spin-orbit-induced manipulation of magnetization vector. Red dashed lines mark easy axes of magnetization. Symmetry of the Dresselhaus spin-orbit field is shown in (b). (For interpretation of the references to color in this figure legend, the reader is referred to the web version of this article.)

substrates. The wafers were subsequently annealed for 1 h at 280 °C in a nitrogen atmosphere, increasing the Curie temperature to $T_c \sim 80$ K and reducing strength of the cubic anisotropy. For the measurements of strain response (Ga,Mn)As layer was patterned into 2 μm -wide Hall bars oriented along the [110] axis by combination of e-beam lithography and wet etching, see Fig. 1(a). After lithography 3 mm \times 3 mm samples were mechanically thinned to ~ 100 μm and attached to a multilayer PZT (piezoelectric lead-zirconium-titanate ceramic) with epoxy, aligning the [010] axis with the axis of polarization of the PZT. Application of positive (negative) voltage V_{PZT} across the piezoelectric introduces tensile (compressive) strain in the sample along the [010] direction, and strain with the opposite sign along the [100] direction proportional to the piezoelectric strain coefficients $d_{33} \approx -2d_{31}$. Both coefficients decrease by a factor of 15 between room temperature and 4.2 K. The induced strain $\varepsilon = \Delta L/L$ for both [010] and [100] directions was monitored with a biaxial strain gauge glued to the bottom of the piezoelectric measured in the Wheatstone bridge configuration: $\Delta\varepsilon = \varepsilon_{[010]} - \varepsilon_{[100]} = (\Delta L/L)_{[010]} - (\Delta L/L)_{[100]} = \alpha(R_{[010]} - R_{[100]})/R$, where α is the gauge sensitivity coefficient and R is the resistance of the unstrained gauge. It has been shown that the strain gradient across the piezoelectric and the sample is negligible: i.e., gauges glued on top of the sample and on the opposite side of the piezoelectric measure similar strain.

For current-induced spin torque experiments, samples were fabricated from 15-nm and 10-nm thick epilayers. The devices were patterned into 6 and 10 μm -diameter circular islands in order to decrease domain pinning. In the following we report data on $\varnothing = 6$ μm devices, other devices show similar results. Cr/Zn/Au (5 nm/10 nm/300 nm) Ohmic contacts were thermally evaporated. All measurements were performed in a variable temperature cryostat at $T = 40$ K, well below the temperature of (Ga,Mn)As-specific cubic-to-uniaxial magnetic anisotropy transitions [16], which is 60 K in the reported wafer. Temperature rise for the largest currents used in the reported experiments was measured to be < 3 K.

In order to determine the direction of magnetization \mathbf{M} , we use the dependence of transverse anisotropic magnetoresistance $R_{xy} = V_y/I_x$ on magnetization [22]:

$$R_{xy} = \Delta\rho \sin \varphi_M \cos \varphi_M,$$

where $\Delta\rho = \rho_{\parallel} - \rho_{\perp}$, $\rho_{\parallel} < \rho_{\perp}$ are the resistivities for magnetization oriented parallel and perpendicular to the current, and $\varphi_M = \angle \mathbf{M}\mathbf{I}$ is an angle between magnetization and current, see Fig. 1(a). In circular samples the current distribution is non-uniform and the angle between the magnetization and the local current density varies throughout the sample. However, it can be shown that the resulting R_{xy} is the same as for a uniform current distribution. For the current-to-current-density conversion, we model our sample as a perfect disk with two point contacts across the diameter. The average current density in the direction of current injection is $\langle j \rangle = 2I/(\pi ad)$, where a is the disk radius and d is the (Ga,Mn)As layer thickness. In a real sample the length of contact overlap with (Ga,Mn)As insures that j changes by less than factor of 3 throughout the sample.

3. Theory

Microscopic physics of transport and magnetism in (Ga,Mn)As system remains controversial to date. There are two competing points of view on what kind of charge carriers are responsible for these properties: (i) whether these are degenerate free holes arising in the Γ_8 valence band, when valence electrons are captured by Mn acceptors, or (ii) these are mobile charge carriers in an impurity band formed by random Mn. However, understanding many physical properties of (Ga,Mn)As require only knowledge of the system symmetry, rather than precise microscopic identification of charge carriers. The key to this understanding is that energy levels of Mn acceptors are centered around 112 meV inside the forbidden gap atop the Γ_8 band, while the gap itself is about 1.5 eV. The physics of the system from the vantage point afforded by symmetry is similar to that in systems

with shallow acceptors, in which symmetry of holes in valence and impurity bands can be largely considered the same [23].

On deeply microscopic level, the charge carrier angular momentum $\mathbf{J}_{3/2}$ is coupled antiferromagnetically to Mn angular momentum $\mathbf{I}_{5/2}$ [24], so that Mn acceptors are described by

$$H_{JI} = A\mathbf{I} \cdot \mathbf{J}. \quad (1)$$

This Hamiltonian together with properties of interactions and spectral and kinetic characteristics of the subsystem of mobile carriers defines the magnetization \mathbf{M} in ferromagnetic (Ga,Mn)As. The single-particle properties of charge carriers with angular momentum 3/2 themselves are described by the Hamiltonian with the following three ingredients.

First, the charge carriers in the absence of external magnetic field but in the presence of strain introduced by Mn doping or externally are characterized by Luttinger–Pikus [25,26] Hamiltonian

$$\mathcal{H}_h = A_0 p^2 + A_1 \sum_i J_i^2 p_i^2 + A_2 \sum_{ij \neq i} J_i J_j p_i p_j + B_1 \sum_i \varepsilon_{ii} J_i^2 + B_2 \sum_{ij \neq i} J_i J_j \varepsilon_{ij}, \quad (2)$$

where $ij = x, y, z$. We use here the notation for the constants in (2), which differs from that for Luttinger constants for zero strain γ_1, γ_2 and γ_3 [25] and constants a, b and d introduced by Bir and Pikus [26] for describing the effects of strain for valence band holes, in order to underscore the applicability of (2) for charge carriers in both the valence and impurity bands.

The second ingredient of the Hamiltonian of charge carriers comes from the effect of magnetization in the crystal

$$\mathcal{H}_{hM} = \mu\kappa \mathbf{J} \cdot \mathbf{M}(\mathbf{r}). \quad (3)$$

In general, \mathbf{M} also couples to the components of axial vector J_i^z , however, these terms are known to be much smaller than the linear coupling term (3). The Hamiltonian (3) implies that holes are affected by magnetic interactions with Mn acceptors via resulting ferromagnetic magnetization, and this effectively allows to consider system of Mn and charge carrier system separately, including only feedback coupling via (1). It is also worth noticing that magnetization of the ferromagnet affects properties of holes only via ferromagnetic coupling (3), but has no effect in orbital channel via (2). This, strictly speaking, makes the effect of magnetization different from that of external magnetic field. The latter affects spin properties not only via coupling (3) but also via the angular momentum–momentum coupling (2), when \mathbf{p} becomes $\mathbf{p} - e\mathbf{A}/c$ in magnetic field, \mathbf{A} is the external magnetic field vector potential.

The third ingredient of the charge carrier Hamiltonian is associated with the absence of inversion symmetry in (Ga,Mn)As system. In the presence of strain, there is an additional angular momentum–momentum coupling

$$\mathcal{H}' = \sum_i C_1 [J_i p_i (\varepsilon_{i+1, i+1} - \varepsilon_{i+2, i+2}) + C_2 (J_i p_{i+1} - J_{i+1} p_i) \varepsilon_{i, i+1}], \quad (4)$$

where cyclic permutation of indices is implied, and for $i=x$ we define $i+1=y$ and $i+2=z$. This Hamiltonian couples angular momentum projections J_i with linear momentum projections, and thereby has symmetry that permits uniform magnetization of the system by an applied electric current. The strain-induced term defined by the constant C_1 has a symmetry similar to that of the Dresselhaus term in two dimensional (2D) electron gas grown along [001] direction, Fig. 1(b). The terms proportional to the constant C_2 arise in the presence of shear strain, and their symmetry is similar to that of Rashba term in 2D electron systems confined by asymmetric potential. We note that there are other terms associated with the lack of inversion symmetry in GaAs, most notably bulk Dresselhaus term that is cubic in momentum [27], and linear

in momentum term that couples to $[J_i, (J_{i+1}^2 - J_{i+2}^2)]_{\text{symm}}$ projections [28]. None of these terms allow polarization of charge carrier spin linear in applied electric current. We also note that in confined geometries, when holes in ground state have heavy mass in the direction of quantization, asymmetric confinement potential does not allow spin Hamiltonian linear in momentum, and does not result in uniform polarization of hole spins linear in applied electric current. In this regard, linear in momentum interaction (4) in bulk GaAs and (Ga,Mn)As system is unique. We underscore that terms associated with shear strain in (4) are unrelated to the structurally induced asymmetry, and only their symmetry reminds the Rashba term that gives spin polarization perpendicular to the flowing current [29,30].

Let us now discuss the symmetry properties and physics of magnetization orientation in (Ga,Mn)As using this model Hamiltonian. The magnetization of the sample provides a preferential direction for angular momentum of holes \mathbf{J} according to (3). In turn, angular momentum of holes has a feedback onto angular momentum \mathbf{I} of Mn acceptors system via (1). In equilibrium, the whole system of holes and acceptors resides at an energy minimum. In this regard, strains in the system are of utmost importance. In GaAs, in the absence of external strain, the internal compressive strain comes from Mn ions, with compressive strain characterized by $\varepsilon_{zz} > 0$ and corresponding volume-preserving strain components $\varepsilon_{xx} = \varepsilon_{yy} < 0$. Then, orientation of \mathbf{J} by \mathbf{M} along z would be energetically unfavorable, while in-plane \mathbf{J} and \mathbf{M} would reduce energy of charge carriers. From the vantage point afforded by the strain itself, all in-plane directions are equivalent, but the hole spectrum is additionally governed by the strain-independent terms, with different constants A_1 and A_2 characterizing the so-called warping, (2). Minimization of hole energy taking warping into account gives four equivalent directions, [100], [010], $[\bar{1}00]$ and $[0\bar{1}0]$ of the preferential orientation of \mathbf{J} and \mathbf{M} . Applied external magnetic field rotated in plane is capable of switching between these four equivalent directions. Furthermore, if we now introduce sufficiently strong external in-plane strain, e.g., making $\varepsilon_{xx} \neq \varepsilon_{yy}$, this applied strain will define only two preferential directions of in-plane orientation of \mathbf{J} and \mathbf{M} .

If the electric current flows through the system, it leads to the orientation of angular momentum of holes via (4). As shown in [20], orientation of angular momentum with electric current comes directly from non-equilibrium distribution of holes by an electric field. In this regard, the orientation of angular momentum of holes differs from polarization of electron spins by the electric current [29,30], when non-equilibrium distribution of holes in applied electric field on its own is insufficient, and spin polarization arises only in the course of spin relaxation. Macroscopically, flowing electric current induces additional component of $\langle \mathbf{J} \rangle$, which direction is defined by both internal and external strain in the (4), and the direction of the flowing current. Application of external magnetic field also results in variation of $\langle \mathbf{J} \rangle$ and is capable of compensating the polarizing effect of the electric current. This allows measurement of the current-induced spin polarization demonstrated below.

4. Results

4.1. Magnetization rotation via strain control

In Fig. 2 R_{xy} is plotted for the strained and unstrained Hall bars as magnetic field of constant magnitude $H=50$ mT is rotated in the plane of the sample. For the unstrained sample (not attached to the piezoelectric), there are four extrema for the external field angles φ_H around $45^\circ, 135^\circ, 225^\circ$ and 315° with four switchings of magnetization by 90° near $[110]$ and $[\bar{1}\bar{1}0]$ axes. For the strained

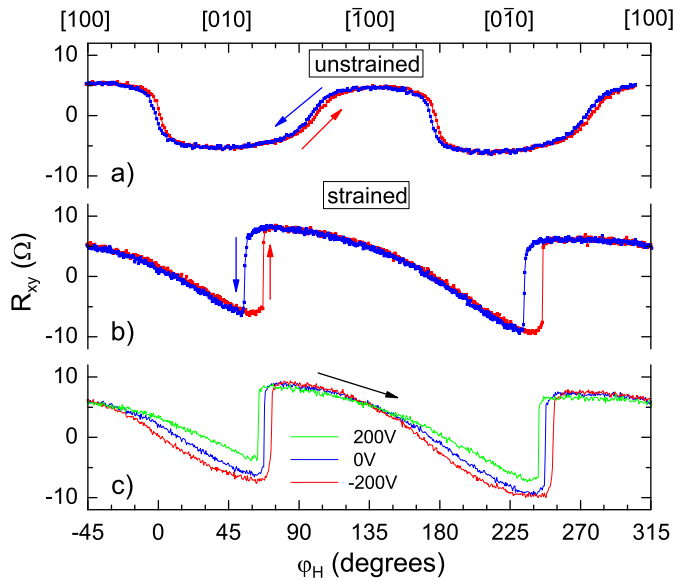


Fig. 2. Transverse anisotropic magnetoresistance (R_{xy}) in unstrained (a) and strained (b) samples for clockwise and counterclockwise rotation of an external magnetic field $H=50$ mT. In (c) R_{xy} for clockwise field rotation is shown with different voltages applied to the PZT.

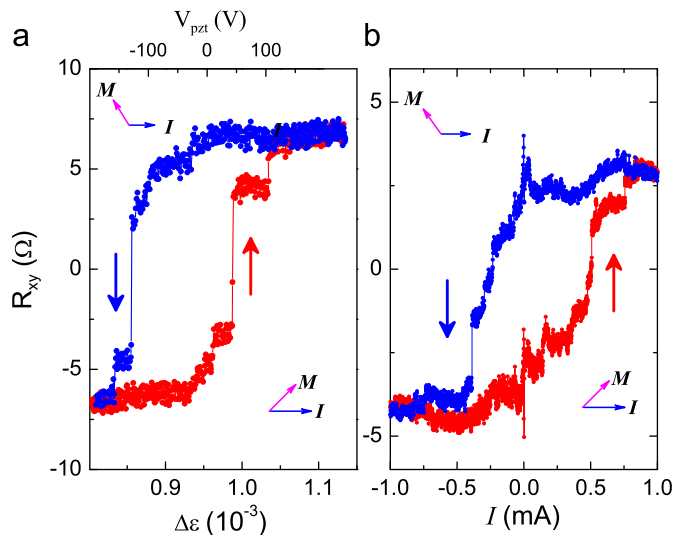


Fig. 3. Hysteretic switching of magnetization as a function of (a) strain and (b) current. In (a) a static magnetic field $H=50$ mT is applied at $\varphi_H=62^\circ$. On the top axis approximate voltage on the PZT is indicated (ignoring small hysteresis in V_{pzt} vs strain). In (b) $H=6$ mT is applied at $\varphi_H=72^\circ$. Orientation of magnetization relative to the current flow is shown schematically for the $R_{xy} > 0$ and $R_{xy} < 0$ states.

sample there is a gradual change in the angle of magnetization with only two abrupt 90° switchings per field rotation, which indicates strong uniaxial anisotropy due to a highly anisotropic thermal expansion coefficient of the PZT stack ($+1$ ppm/K along and -3 ppm/K perpendicular to the piezoelectric stack).

Application of $H=50$ mT at $\varphi_H=62^\circ$ compensates the thermally induced uniaxial strain and restores the original degeneracy between $[010]$ and $[\bar{1}00]$ magnetization directions of the unstrained (Ga,Mn)As for $V_{pzt} \approx 0$. An additional strain is then applied by varying voltage on the piezoelectric. In Fig. 3(a) R_{xy} is plotted as a function of measured strain $\Delta\epsilon$, the corresponding V_{pzt} are approximately marked on the top axis (there is a small hysteresis in $\Delta\epsilon$ vs V_{pzt}). As additional compressive strain is applied along $[010]$, this direction becomes the easy axis of

magnetization and magnetization aligns itself with $[010]$. As additional tensile strain is applied along $[010]$ direction, the $[\bar{1}00]$ direction becomes the easy axis and polarization switches by 90° . The switching occurs in a few steps, indicating a few-domain composition of our device. At $V_{pzt}=0$ the magnetization has two stable orientations, $\vec{M} \parallel [\bar{1}00]$ and $\vec{M} \parallel [010]$, and the orientation can be switched by applying a negative or a positive voltage on the piezoelectric. Thus, the device performs as a bi-stable non-volatile magnetic memory with electrostatic control of the state.

The center of the hysteresis loop in Fig. 3(a) can be shifted by adjusting φ_H : e.g., a 1° change shifts the center of the loop by $\Delta\epsilon \approx 3.5 \times 10^{-5}$. As H increases, the size of the hysteresis loop decreases, and the hysteresis vanishes for $H > 100$ mT. At $H < 40$ mT the loop increases beyond the accessible ± 200 V voltage span. In our experiments the magnetic field balances the residual strain due to anisotropic thermal expansion of the PZT.

4.2. Magnetization rotation via spin-orbit interaction

In the presence of a strong external magnetic field \mathbf{H} , the magnetization of the ferromagnetic island is aligned with the field. For weak fields, however, the direction of magnetization is primarily determined by magnetic anisotropy. As a small field ($5 < H < 20$ mT) is rotated in the plane of the sample, the magnetization is re-aligned along the easy axis closest to the field direction. Such rotation of magnetization in circular samples (Fig. 1(b)) by an external field is shown in Fig. 4(a). For the current $\mathbf{I} \parallel [\bar{1}10]$, the measured R_{xy} is positive for $\mathbf{M} \parallel [100]$ and negative for $\mathbf{M} \parallel [010]$. Note that R_{xy} , and thus also the magnetization, switches direction when the direction of \mathbf{H} is close to the hard axes $[110]$ (φ_H^0 and $\varphi_H^{180^\circ}$) and $[\bar{1}10]$ ($\varphi_H^{90^\circ}$ and $\varphi_H^{270^\circ}$), confirming the cubic magnetic anisotropy of our samples.

In the presence of both external and current-induced spin-orbit magnetic fields, we expect to see a combined effect of $\mathbf{H} + \mathbf{H}^{so}$ on the direction of the magnetization. For small currents (few μA) $H^{so} \approx 0$, and R_{xy} does not depend on the sign or the direction of the current. At large dc currents the value of the switching angle becomes current-dependent and we define $\Delta\varphi_H(I) = \varphi_H(+I) - \varphi_H(-I)$. Specifically, for $\mathbf{I} \parallel [\bar{1}10]$ the switching of magnetization around $\varphi_H = 90^\circ$ ($[010] \rightarrow [\bar{1}00]$) occurs for $I = +0.7$ mA at larger angles than for $I = -0.7$ mA, $\Delta\varphi_H^{90^\circ} > 0$. For the switching near $\varphi_H = 270^\circ$ ($[0\bar{1}0] \rightarrow [100]$) the I -dependence of switching angle is reversed, $\Delta\varphi_H^{270^\circ} < 0$. There is no measurable difference in the switching angle for magnetization switching around $\varphi_H = 0^\circ$ and 180° ($[100] \rightarrow [010]$ and $[\bar{1}00] \rightarrow [0\bar{1}0]$), $\Delta\varphi_H^0, \Delta\varphi_H^{180^\circ} \approx 0$. When the current is rotated by 90° ($\mathbf{I} \parallel [110]$), we observe $\Delta\varphi_H^0 > 0$, $\Delta\varphi_H^{180^\circ} < 0$, and $\Delta\varphi_H^{90^\circ}, \Delta\varphi_H^{270^\circ} \approx 0$.

The data can be qualitatively understood if we consider an additional current-induced effective magnetic field \mathbf{H}^{eff} . In the absence of \mathbf{H}^{eff} magnetization rotation occurs when external field \mathbf{H} is aligned with a hard axes. In the presence of $\mathbf{H}^{eff} \neq 0$ rotation is initiated when the total field $\mathbf{H}^{tot} = \mathbf{H} + \mathbf{H}^{eff}$ is aligned with the hard axes. Depending on the direction of \mathbf{H}^{eff} the switching angle becomes large, smaller or is not effected by \mathbf{H}^{eff} , as shown schematically in Fig. 4(b) for $\mathbf{I} \parallel [\bar{1}10]$.

The dependence of $\Delta\varphi_H$ for different magnitudes and directions of the current is summarized in Fig. 4(c) and (d). Assuming that the angle of magnetization switching depends only on the total field \mathbf{H}^{tot} , we can extract the magnitude H^{eff} and the angle $\theta = \angle \mathbf{I} \mathbf{H}^{eff}$ from the measured $\Delta\varphi_H$, thus reconstructing the whole vector \mathbf{H}^{eff} . Taking into account that $\Delta\varphi_H$ is small, we find that

$$H^{eff} \approx H \sin(\Delta\varphi_H/2) / \sin(\theta - \varphi_H)$$

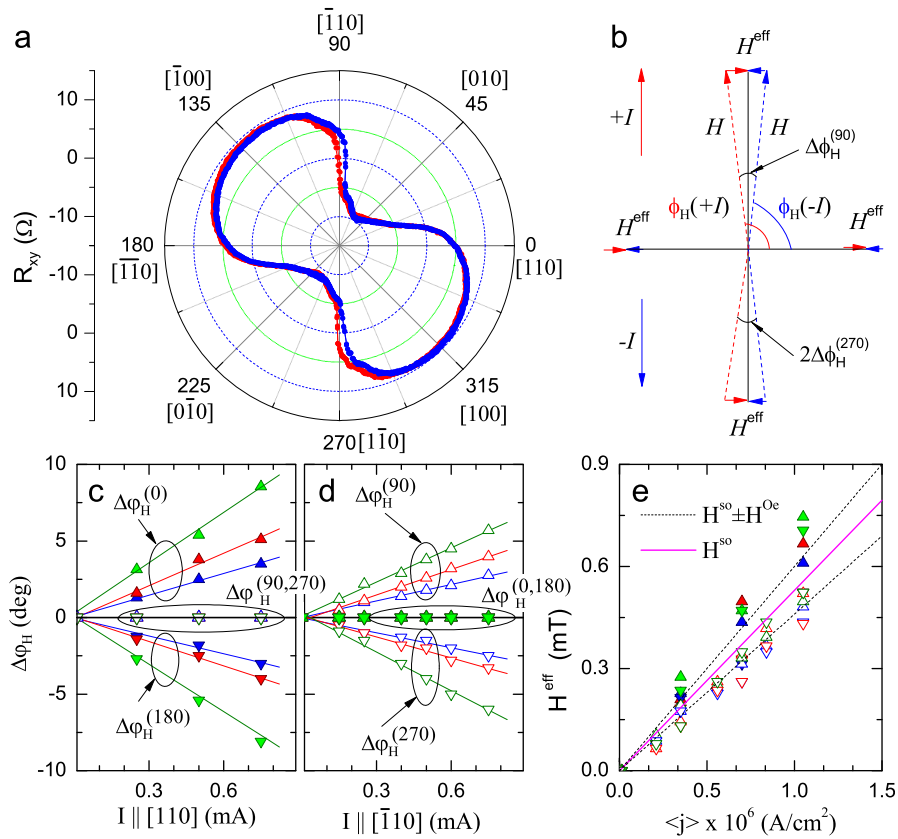


Fig. 4. (a) Transverse anisotropic magnetoresistance is plotted as a function of external magnetic field angle φ_H in the presence of a dc current $I = \pm 0.7$ mA, $I \parallel [\bar{1}10]$. In (b) the change of the switching angle $\varphi_H(\pm I)$ in the presence of current-induced effective field H^{eff} is shown schematically. In (c,d) a difference between switching angles $\Delta\varphi_H = \varphi_H(+I) - \varphi_H(-I)$ is summarized for different current values and directions. (e) Effective field is extracted from (c,d) and is plotted as a function of average current density. The solid line is the actual dependence of spin-orbit field H^{so} after correction for the current-induced Oersted field H^{Oe} .

and θ can be found from the comparison of switching at two angles. We find that $\theta \approx 90^\circ$, or $\mathbf{H}^{\text{eff}} \perp \mathbf{I}$ for $I \parallel [110]$ and $I \parallel [\bar{1}10]$. Moreover, the symmetry of the measured \mathbf{H}^{eff} with respect to \mathbf{I} coincides with the unique symmetry of the strain-related SO field characterized by the constant C_1 in (4) and depicted in Fig. 1(b).

In Fig. 4(e), H^{eff} is plotted as a function of the average current density $\langle j \rangle$. There is a small difference in the H^{eff} vs $\langle j \rangle$ dependence for $I \parallel [110]$ and $I \parallel [\bar{1}10]$. As shear strain is not present in our samples, and the term proportional to the constant C_2 in (4) vanishes, the difference can be explained by considering the current-induced Oersted field $H^{\text{Oe}} \propto I$ in metal contacts. The Oersted field is localized under the pads, which constitutes $\sim 7\%$ of the sample. The Oersted field has the same symmetry as that of the field described by the terms with the constant C_2 in (4) and is added to or subtracted from the SO field depending on the current direction. Thus, $H^{\text{eff}} = H^{\text{so}} + H^{\text{Oe}}$ for $I \parallel [110]$ and $H^{\text{eff}} = H^{\text{so}} - H^{\text{Oe}}$ for $I \parallel [\bar{1}10]$. We estimate the fields to be as high as 0.6 mT under the contacts at $I = 1$ mA, which corresponds to $H^{\text{Oe}} \approx 0.04$ mT averaged over the sample area. These estimates are reasonably consistent with the measured values of 0.07 mT. Finally, we determine H^{so} as an average of H^{eff} between the two current directions. The SO field depends linearly on j , as expected for strain-related SO interactions: $dH^{\text{so}}/dj = 0.53 \times 10^{-9}$ T cm²/A. This result is in agreement with quantitative theoretical calculation of orientation of hole spins by current in [20].

Current-induced effective SO field H^{so} is sufficient to reversibly manipulate the direction of magnetization. If we fix $H = 6$ mT at $\varphi_H = 72^\circ$, R_{xy} forms a hysteresis loop as current is swept between ± 1 mA, as shown in Fig. 3(b). R_{xy} is changing between

$\pm 5 \Omega$, indicating that \mathbf{M} is switching between $[010]$ and $[\bar{1}00]$ directions.

5. Conclusions

We demonstrated that the vector of ferromagnetic magnetization can be manipulated by inducing anisotropy into the spectra of holes in (Ga,Mn)As by application of uniaxial strain or current-induced polarization of holes via spin-orbit interactions, and explained these effects based on symmetry analysis. In both cases the devices perform as a non-volatile memory cells, with two states encoded in the magnetization direction. The direction can be controlled by application of an external strain or an unpolarized current passing through the device. Devices can be potentially operated as a four-state memory cells. We find that we can reversibly switch the magnetization with currents as low as 0.5 mA (current densities 7×10^5 A/cm²), an order of magnitude smaller than by polarized current injection in ferromagnetic metals [6,7,31], and just a few times larger than by externally polarized current injection in ferromagnetic semiconductors [32]. In current experiments PZT material has few- μF capacitance, which precludes high frequency operation. However, one can utilize piezoelectric properties of GaAs. In GaAs d_{14} shear coefficient is 100 times smaller than d_{33} coefficient for PZT, but similar strain can be achieved in thin GaAs layers well below the breakdown voltage. The use of nanofabrication will allow capacitance reduction down to a few pF, which will enable high frequency magnetization control.

Acknowledgments

Y.L.G. acknowledges support by NSF Grant ECCS-0901754.

References

- [1] S.A. Wolf, D.D. Awschalom, R.A. Buhrman, J.M. Daughton, S.V. Molnar, M.L. Roukes, A.Y. Chtchelkanova, D.M. Treger, Spintronics: a spin-based electronics vision for the future, *Science* 294 (2001) 1488–1495.
- [2] M. Baibich, J. Broto, A. Fert, F. Nguyen Van Dau, F. Petroff, P. Etienne, G. Creuzet, A. Friederich, J. Chazelas, Giant magnetoresistance of (001)Fe/(001)Cr magnetic superlattices, *Physical Review Letters* 61 (1988) 2472–2475.
- [3] G. Binasch, P. Grünberg, F. Saurenbach, W. Zinn, Enhanced magnetoresistance in layered magnetic structures with antiferromagnetic interlayer exchange, *Physical Review B* 39 (1989) 4828–4830.
- [4] J. Moodera, L. Kinder, T. Wong, R. Meservey, Large magnetoresistance at room temperature in ferromagnetic thin film tunnel junctions, *Physical Review Letters* 74 (1995) 3273–3276.
- [5] G.A. Prinz, Magneto-electronics, *Science* 282 (1998) 1660–1663.
- [6] J.C. Slonczewski, Current-driven excitation of magnetic multilayers, *Journal of Magnetism and Magnetic Materials* 159 (1996) 1–7.
- [7] L. Berger, Emission of spin waves by a magnetic multilayer traversed by a current, *Physical Review B* 54 (1996) 9353–9358.
- [8] J. Gaj, J. Ginter, R. Galazka, Exchange interaction of manganese $3d^5$ states with band electrons in $Cd_{1-x}Mn_xTe$, *Physica Status Solidi B* 89 (1978) 655–662.
- [9] M. Jaczynski, J. Kossut, R. Galazka, Influence of exchange interaction on the quantum transport phenomena in $Hg_{1-x}Mn_xTe$, *Physica Status Solidi B* 88 (1978) 73–85.
- [10] H. Ohno, A. Shen, F. Matsukura, A. Oiwa, A. Endo, S. Katsumoto, Y. Iye, (Ga,Mn)As: a new diluted magnetic semiconductor based on GaAs, *Applied Physics Letters* 69 (1996) 363–365.
- [11] H. Ohno, Making nonmagnetic semiconductors ferromagnetic, *Science* 281 (1998) 951–956.
- [12] D.V. Baxter, D. Ruzmetov, J. Scherschligt, Y. Sasaki, X. Liu, J.K. Furdyna, C.H. Mielke, Anisotropic magnetoresistance in $Ga_{1-x}Mn_xAs$, *Physical Review B* 65 (2002) 212407.
- [13] T. Jungwirth, J. Sinova, J. Masek, J. Kucera, A.H. MacDonald, Theory of ferromagnetic (III,Mn)V semiconductors, *Reviews of Modern Physics* 78 (2006) 809–846.
- [14] H. Ohno, D. Chiba, F. Matsukura, T. Omiya, E. Abe, T. Dietl, Y. Ohno, K. Ohtani, Electric-field control of ferromagnetism, *Nature* 408 (2000) 944–946.
- [15] I. Stolichev, S.W.E. Riester, H.J. Trodahl, N. Setter, A.W. Rushforth, K.W. Edmonds, R.P. Campion, C.T. Foxon, B.L. Gallagher, T. Jungwirth, Non-volatile ferroelectric control of ferromagnetism in (Ga,Mn)As, *Nature Materials* 7 (2008) 464–467.
- [16] D. Chiba, M. Sawicki, Y. Nishitani, Y. Nakatani, F. Matsukura, H. Ohno, Magnetization vector manipulation by electric fields, *Nature* 455 (2008) 515–518.
- [17] A.M. dos Santos, S. Parashar, A.R. Raju, Y.S. Zhao, A.K. Cheetham, C.N.R. Rao, Evidence for the likely occurrence of magnetoferroelectricity in the simple perovskite, $BiMnO_3$, *Solid State Communications* 122 (2002) 49–52.
- [18] M. Murakami, S. Fujino, S.-H. Lim, C.J. Long, L.G. Salamanca-Riba, M. Wuttig, I. Takeuchi, V. Nagarajan, A. Varatharajan, Fabrication of multiferroic epitaxial $BiCrO_3$ thin films, *Applied Physics Letters* 88 (2006) 152902.
- [19] M. Sakai, A. Masuno, D. Kan, M. Hashisaka, K. Takata, M. Azuma, M. Takano, Y. Shimakawa, Multiferroic thin film of Bi_2NiMnO_6 with ordered double-perovskite structure, *Applied Physics Letters* 90 (2007) 072903.
- [20] A. Chernyshov, M. Overby, X. Liu, J.K. Furdyna, Y. Lyanda-Geller, L.P. Rokhinson, Evidence for reversible control of magnetization in a ferromagnetic material by means of spin-orbit magnetic field, *Nature Physics* 5 (2009) 656–659. doi:10.1038/nphys1362.
- [21] M. Overby, A. Chernyshov, L.P. Rokhinson, X. Liu, J.K. Furdyna, GaMnAs-based hybrid multiferroic memory device, *Applied Physics Letters* 92 (2008) 192501. doi:10.1063/1.2917481.
- [22] H.X. Tang, R.K. Kawakami, D.D. Awschalom, M.L. Roukes, Giant planar hall effect in epitaxial (Ga,Mn)As devices, *Physical Review Letters* 90 (2003) 107201.
- [23] B.I. Shklovskii, A.L. Efros, *Electronic Properties of Doped Semiconductors*, Springer-Verlag, New York, 1994.
- [24] I. Karlik, I. Merkulov, D. Mirlin, L. Nikitin, V. Perel', V. Sapega, Magnetization of holes at acceptors and the polarization of the hot photoluminescence in GaAs:Mn crystals, *Soviet Physics—Solid State* 24 (1983) 2022–2026.
- [25] J.M. Luttinger, Quantum theory of cyclotron resonance in semiconductors: general theory, *Physical Review* 102 (1956) 1030–1041.
- [26] G. Pikus, G. Bir, Effect of deformation on the hole energy spectrum of germanium and silicon, *Soviet Physics—Solid State* 1 (1960) 1502–1517.
- [27] G. Dresselhaus, Spin-orbit coupling effects in zinc blende structures, *Physical Review* 100 (1955) 580–586.
- [28] G.L. Bir, G.E. Pikus, *Symmetry and Strain-induced Effects in Semiconductors*, Wiley, New York, 1974.
- [29] A.G. Aronov, Y.B. Lyanda-Geller, Nuclear electric resonance and orientation of carrier spins by an electric field, *JETP Letters* 50 (1989) 431–434.
- [30] A.G. Aronov, Y.B. Lyanda-Geller, G.E. Pikus, Spin polarization of electrons by an electric current, *Soviet Physics JETP* 73 (1991) 537–541.
- [31] E.B. Myers, D.C. Ralph, J.A. Katine, R.N. Louie, R.A. Buhrman, Current-induced switching of domains in magnetic multilayer devices, *Science* 285 (1999) 867–870.
- [32] D. Chiba, Y. Sato, T. Kita, F. Matsukura, H. Ohno, Current-driven magnetization reversal in a ferromagnetic semiconductor (Ga,Mn)As/GaAs/(Ga,Mn)As tunnel junction, *Physical Review Letters* 93 (2004) 216602.